Research Article Vol. 32, No. 6 / 11 Mar 2024 / Optics Express 9767
Optics EXPRESS

High efficiency diode-pumped Pr:$LiLuF_4$ visible lasers in femtosecond-laser-written waveguides

DAVIDE BAIOCCO,[1,*] IGNACIO LOPEZ-QUINTAS,[2] JAVIER R. VÁZQUEZ DE ALDANA,[2] MAURO TONELLI,[1] AND ALESSANDRO TREDICUCCI[1]

[1]*Dipartimento di Fisica, Universitá di Pisa, Largo Bruno Pontecorvo 3, 56127 Pisa PI, Italy*
[2]*Grupo de Investigación en Aplicaciones del Láser y Fotánica, Universidad de Salamanca, Pl. La Merced SN. 37008 Salamanca, Spain*
[*]*davide.baiocco@phd.unipi.it*

Abstract: In this work we investigate the power scaling of diode-pumped Pr:$LiLuF_4$ waveguide lasers produced by direct femtosecond writing. The waveguides studied consisted in depressed cladding waveguides with different geometries. We observed laser emission at 604 nm, achieving a maximum output power of 275 mW and a slope efficiency of 40%, and 721 nm, demonstrating 310 mW of output power and a slope efficiency of 50%. Moreover, we obtained, what we believe is for the first time in a diode-pumped waveguide, laser emission at 523 nm, with a maximum output power of 65 mW and a slope efficiency of 11%. In the end, we also demonstrated the first diode-pumped operation of a single-transverse-mode waveguide laser at 721 nm, reaching a maximum output power of 28 mW and maintaining a high quality beam with an M^2 of 1.1.

1. Introduction

Visible lasers are commonly employed in many aspects of scientific research and everyday life, leading to the necessity of miniaturization of such devices. Nowadays, the two leading technologies for the construction of visible lasers are laser diodes and solid state lasers (SSLs). SSLs possess the advantage of a smaller emission bandwidth with respect to laser diodes and an intrinsic long term stability, thus reducing the frequency noise and totally preventing the wavelength drift induced by aging [1], both attractive features for metrological devices. In addition, the beam emitted by a SSL is typically quasi-diffraction-limited, allowing easier focusing and simplifying the application of the laser in more complex systems. An ion that has been intensively studied for the fabrication of laser devices directly operating in the visible range is praseodymium. Trivalent praseodymium possesses strong emission lines in all the visible range: cyan (480 nm), green and orange (520 nm and 605 nm), red and deep red (640 nm and 720 nm).

Fluoride crystals are an optimal host for Pr^{3+} due to their lower phonon energy, which suppresses the nonradiative decay of excited states, and the higher energy difference between $4f^2$ and 4f5d states, which impedes excited state absorption both at the laser and at the pump wavelengths [2,3]. Moreover, Pr-doped fluorides demonstrated the possibility of laser emission at all the fundamental lines necessary for the operation of Sr-based atomic clocks [4]. Other advantages of this class of materials are their resistance in chemically severe conditions and their non-hygroscopicity, both appealing features for the fabrication of robust devices. Pr-based lasers have been intensively studied in recent years, after the demonstration and the development of the blue-emitting InGaN-based laser diodes, today commercially available with output power reaching several Watt. They can be employed, in fact, as pump sources for the excitation of Pr ions, since their emission region matches the $^3H_4 \rightarrow {}^3P_2$ absorption band in many different hosts [2].

#516789 https://doi.org/10.1364/OE.516789
Journal © 2024 Received 21 Dec 2023; revised 29 Jan 2024; accepted 29 Jan 2024; published 4 Mar 2024

Optics EXPRESS

Several attempts have been made to reduce the dimensions of the external cavity of the SSLs. In particular, Davis et al demonstrated that it is possible to modify the refractive index of a material by irradiating it with ultrashort laser pulses [5]. Many works have then been published showing waveguided laser emission in the near infrared region, by exploiting the lines of Nd [6], Tm [7], and Yb (both continuous wave [8] and pulsed [9,10]), but only a few concerning visible waveguide lasers based on Pr ions, since shorter wavelengths require materials with higher optical quality and waveguides with lower propagation losses. [11–17].

The aim of this work is to demonstrate that it is possible to develop all-solid-state compact visible lasers with high efficiency and relatively low cost. The use of a laser diode, compared to other commercially available pump sources, such as the 2ω-OPSL [3], allows the reduction of the size of the active device, thereby increasing its reliability, stability, and lifetime. We report for the first time on the power scaling of a diode pumped Pr-based waveguide laser created by femtosecond laser writing. In this framework, we demonstrated slope efficiencies at 604 nm and 721 nm comparable to those reported for bulk Pr-based lasers operating at these wavelengths. Moreover, we obtained the first operation of a diode-pumped waveguide laser in the green region (523 nm).

2. Material growth and waveguide fabrication

To build the waveguide laser, we chose to work with Pr-doped $LiLuF_4$ (LLF). The choice of this crystal matrix was favored by its advantages when compared to other fluorides. LLF is a tetragonal crystal with a scheelite-like structure [18], resulting thus isomorph to the common $LiYF_4$ (YLF). With respect to YLF though, LLF shows better thermomechanical properties [19], a lower effective phonon energy [20] and can be grown from a congruent melt, potentially resulting in crystals with a better optical quality. The anisotropic nature of the host reflects in the optical behavior of the doped crystal. In fact, the crystal is uniaxial, with a difference between ordinary refractive index and extraordinary refractive index of about 0.02 [21]. Absorption and emission spectra of Pr ions depend both on the light polarization. In this host, the $^3H_4 \rightarrow {}^3P_2$ absorption transition of Pr^{3+} ions is located at 444 nm for π-polarization(E//c), with an absorption cross section of about $10^{-19}cm^2$. Concerning fluorescence, a strong emission line is present at about 480 nm for π polarization, while different green lines can be found between 523 nm and 550 nm. In the "orange" part of the spectrum a couple of lines can be found at 604 nm(π) and 607 nm (σ). Laser emission at both wavelengths suffers from slight reabsorption due to the presence of the $^3H_4 \rightarrow {}^1D_2$ absorption transition, centered at 597 nm, but this effect does not prevent the operation of high efficiency lasers working at these wavelengths [3]. Regarding red and deep red emissions, three other main lines are present: 640 nm(σ), 698 nm(π), and 721 nm(π). In relation to the emission wavelengths listed before, we report the complete fluorescence spectrum of Pr ions in Fig. 1.

Pr:LLF single crystals were grown by Czochralski growth at the University of Pisa from high purity LiF, LuF_3 and PrF_3 powders. The dopant concentration in the melt was 1%. After the growth, we oriented the boule by X-ray backscattering Laue technique, in order to cut oriented samples. Due to segregation effects [18], the actual dopant concentration in the crystal is different from the melt one. To obtain the real dopant concentration, we measured the absorption coefficient of Pr:LLF single crystals with a CARY 5000 spectrophotometer and we estimated the dopant concentration through the absorption cross sections available in the literature [2]. The estimated value is of 0.2%, in agreement with the one obtained in [18] by ICP analysis. The polarized absorption spectrum is reported in Fig. 2.

For the experiments, we carved and polished a sample with dimensions of 4 mm(a) ×9 mm(a)×4 mm(c), in order to produce 9 mm-long waveguides.

The waveguides were inscribed in the sample by using an amplified Ti:Sapphire laser system (Spitfire, Spectra Physics) that emits pulses with a temporal duration of 60 fs and a central

Optics EXPRESS

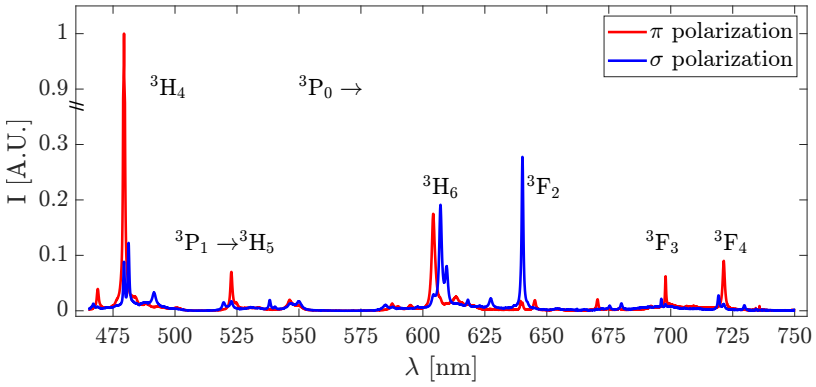

Fig. 1. Polarized fluorescence spectrum of Pr:LLF. The resolution was set to 0.13 nm.

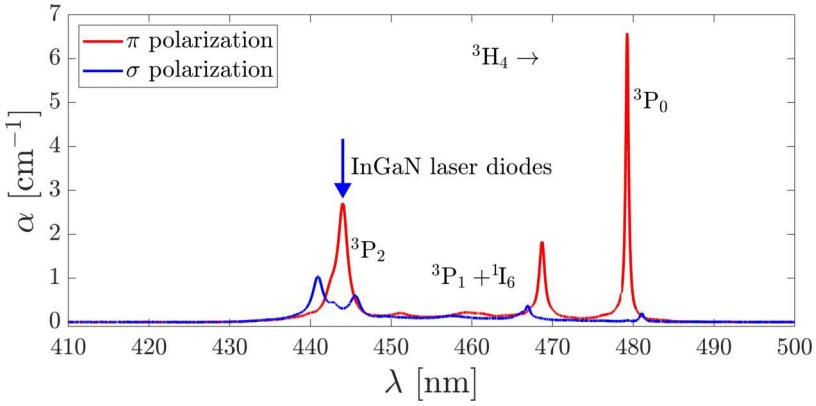

Fig. 2. Polarized absorption spectrum of Pr:LLF. The resolution was set to 0.09 nm. The different absorption transitions are reported nearby the peaks.

wavelength of 800 nm, at a repetition rate of 5 kHz. The pulse energy was controlled by a set of neutral density filters and variable attenuator (half-wave plate and linear polarizer) prior to be focused by a 40× (Leica N-PLAN, N.A. 0.60) microscope objective beneath the sample surface. The motion of the sample was controlled by a XYZ micro-positioning stage (with rotation, tip and tilt manual fine adjustment) in order to produce localized micro-modifications following the required geometry. Under our experimental conditions, the threshold to create micro-modifications in the bulk of the crystal visible with a white-light microscope was around 48 nJ. We fabricated and characterized different waveguide designs [22], varying from weak modifications of the material (Type I) to severe ones (Type II). The best results reported in this work, have been achieved with two depressed cladding waveguides [6] using Type II modification. The first one is a circular cladding waveguide with a diameter of 20 µm (WG1 in the following), while the second one is a circular cladding waveguide with a diameter of 40 µm and some additional tracks on the sides of the waveguide (WG2) to improve the confinement [23]. For the fabrication of both waveguides, a pulse energy of 70 nJ was employed and consisted of parallel damage tracks inscribed with a scanning velocity of 600 µm and a lateral separation between them of 2 µm. The polarization of the laser was kept perpendicular to the c-axis of the crystal.

Optics EXPRESS

3. Waveguide characterization

The first analysis we performed on the waveguides is the estimation of propagation losses by coupling in the waveguides a test beam. The first wavelength tested was 633 nm, using an unpolarized He-Ne laser and a Glan-Thompson polarizer to obtain a polarized beam. To execute the measurements, we placed the crystal in a temperature stabilized copper holder, the same that will be used for laser experiments. We rotated the crystal to have the facet through which the waveguides were written in direct contact with the copper holder to improve the heat exchange. To achieve the best heat dissipation possible, we interposed between the crystal and the copper holder an indium foil. The whole system was placed on a positioning stage composed by a two-axes translation system and a three-axes goniometer, to ensure the best coupling between the incident beam and the waveguide. Coupling and collection optics were mounted in two independent three-axes precision translation stages (Thorlabs MBT616D/M). As collection optics, we employed a microscope objective (Olympus PLN 20×, N.A. 0.4), while we tested different coupling lenses to find the optimal coupling, achieved using an aspherical lens with 30 mm focal length.

The waveguides show good confinement in the core for π polarization while σ polarization is confined in the cladding. We also checked the presence of a single or multiple guided modes by imaging the beam exiting from the waveguide on a CCD. The 10 µm-radius waveguide (WG1) resulted single mode at this wavelength, while WG2 was found to be multimodal. The pictures of WG1 and WG2, together with the intensity profiles are reported in Fig. 3. From these measurements, it is possible to set an upper limit for the propagation losses of each waveguide, assuming the complete coupling of the incident beam in the waveguide. The best result has been achieved with waveguide WG2, showing a value of 0.2 dB/cm, comparable with the one found in [16,17] for a waveguide with similar geometry and in [15] for ultra-large area waveguides. Concerning WG1, the upper limit for propagation losses is 2.2 dB/cm. This value, an order of magnitude greater than the one observed in the multimodal waveguide, contains the contribution of the coupling losses, and a more stringent value will be obtained from the laser experiment.

A rough estimation of the refractive index change in the irradiated area can be derived from the measurement of the numerical aperture (N.A.) of the waveguide by exploiting the step-index-fiber approximation [7]. We measured the N.A. of the waveguide by acquiring the profile of the beam exiting from the waveguide with a CCD camera at different distances from the crystal facet. We carried out the measurement on the WG2 waveguide with π polarized 633 nm radiation, since the high coupling efficiency reduces the scattered light and, thus, the noise of the measurement. With a N.A. of about 0.03 and a refractive index of the core of about 1.5, the refractive index change is about $\Delta n = 2 \times 10^{-4}$, a value comparable with the one reported in [24] for femtosecond laser writing in fluoride crystals. To measure the losses at a shorter wavelength, we repeated the coupling and transmission measurements using a high quality laser diode (Cobolt MLD 405 nm, $M^2 = 1.1$) operating at 405 nm. Contrary to what happens in the 445 nm band, Pr ions do not show absorption at this wavelength and it is possible to set the upper limit without being affected by the ions absorption. The anisotropic behavior observed at 633 nm was confirmed at this second wavelength, with only π polarization confined in the core. The measured upper limit for the propagation losses is 5 dB/cm for WG1 and 0.6 dB/cm for WG2. The third wavelength studied is 444 nm, corresponding to the absorption peak of Pr ions. The source was an InGaN-based laser diode, tuned to emit at the pump wavelength. The output beam was collected by a collimator and shaped with a pair of cylindrical lenses (Schäfter+Kirchhoff 5 AN-3-V-35). Then, the polarization of the beam was controlled with a half wavelength plate (HW) and the power of the beam was regulated with a variable attenuator (VA). The maximum power achieved in front of the coupling lens was of 2.5 W. This laser beam will be used both for coupling and transmission measurement and for pumping Pr ions for laser experiments. Also for this wavelength the waveguides confine only π polarization, while σ polarization is confined in the cladding. Concerning the number of

Optics EXPRESS

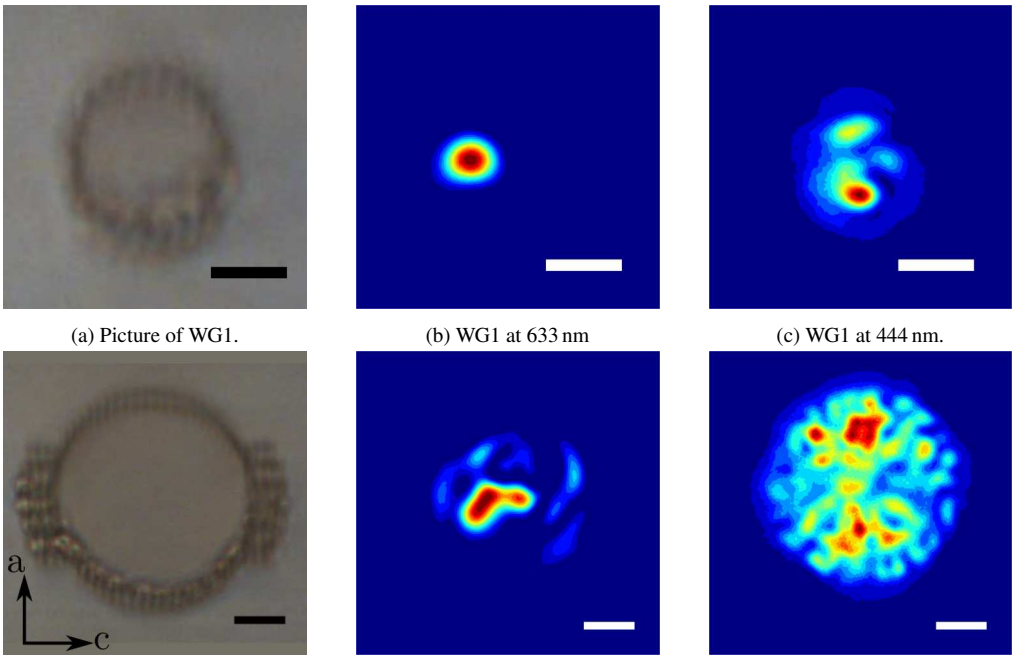

(a) Picture of WG1. (b) WG1 at 633 nm (c) WG1 at 444 nm.

(d) Picture of WG2. (e) WG2 at 633 nm. (f) WG2 at 444 nm.

Fig. 3. Pictures of WG1 (3a) and WG2 (3d) and relative intensity profiles at 633 nm (3b and 3e) and 444 nm (3c and 3f). The intensity profiles have been recorded at maximum coupling efficiency. The scale bar corresponds to 10 µm in all the pictures and the axes depicted in Figuire 3d are common to all pictures.

guided modes, all waveguides show a multimodal behavior. We tested different lenses to find the best coupling efficiency and the lens that showed the best results is the 30 mm focal-length lens previously described.

We measured the parameters of the focused beam obtained with the 30 mm lens by measuring the intensity profile of the beam at different distances from the lens. The beam diameter resulted to be 60 µm with an M^2 of 20 in the horizontal direction while the diameter is 40 µm and the M^2 is 1.7 in the vertical direction. Due to saturation of pump absorption [7,16,17], it is possible to separate coupling efficiency η_{CL} and propagation losses by measuring the transmission efficiency at different values of the incident power. The global best performance has been observed testing WG2, demonstrating a coupling efficiency of 38%. By testing WG1, we achieved a coupling efficiency of 6%. The intensity profiles of the confined modes at 444 nm are reported in Fig. 3(c) (WG1) and 3(f) (WG2). The limiting factor for the coupling efficiency is the numerical aperture of the waveguide, which reflects in a limitation of the incident beam divergence. This affects the minimum diameter of the pump beam and, consequently, the maximum coupling efficiency reachable.

Since it is possible to measure the coupling efficiency, both the threshold power (P_{THR}) and the slope efficiency ($\eta_C = \frac{dP_{OUT}}{dP_c}$) were given as a function of the pump power coupled in the waveguide (P_C). Here P_{OUT} indicates the laser output power.

4. Laser experiments

To build the cavity of the waveguide laser, we placed two flat mirrors in contact with the crystal facets, since the lateral confinement is given by the waveguide. We mounted the mirrors in two

Optics EXPRESS

positioning systems composed by a three-axes translation stage and a two-axes mirror mount, to control position and tilting of each mirror. The structural part of the cavity, composed by mirror holders and sample holder, has been carefully designed to improve mechanical and thermal stability of the whole system, which allows better performances of the waveguide laser. We employed different dielectric mirrors to select the operation wavelength of the waveguide laser. In particular, to study the emission at 523 nm and 721 nm, it is necessary to use input and output couplers designed to suppress lasing at 604 nm, since the $^3P_0 \rightarrow ^3H_6$ transition has the highest emission cross section among π-polarized emission lines [2]. The complete list of mirrors employed for the various experiments is reported in Table 1.

Table 1. Summary of the characteristics of the employed mirrors. The transmittance values were measured with the CARY 5000 spectrophotometer. IC stands for input coupler while OC is the output coupler

Mirror	Use	Transmittance [%] at λ [nm]				
		444	523	604	698	721
1	IC	91	0.005	65	90	85
2	IC	98	93	0.1	<0.001	<0.001
3	OC	97	1	71	92	77
4	OC	6	3	16	58	71
5	OC	9	98	96	69	46

To couple the pump beam in the waveguides we used the 30 mm-focal-length lens (FL) discussed in the previous section and we cooled down the crystal holder to 17°C to ensure the cooling of the sample while preventing moisture condensation. As collection lens (CLL), we used an aspherical lens with a focal length of 20 mm and we removed the residual pump with a dielectric filter (LP). After the dielectric filter, we placed alternatively the power meter, the ModeMaster (Coherent ModeMaster MM-2S beam analyzer, to measure the M^2 of the laser beam) or the CCD camera, the last one placed in the conjugate plane of the crystal facet, in order to acquire the intensity profile of the beam. Imaging in the conjugate plane of the crystal facet and the use of the ModeMaster are fundamental for the characterization of a gaussian laser beam, providing the transverse intensity profile and the values of M^2 for both principal axes of the beam. This allows to avoid an erroneous assessment of beam quality that can derive from a measurement carried out only with a CCD in the far field.

A schematic of the laser cavity is reported in Fig. 4. During all the experiments, the emission spectrum of the laser was checked with a QEpro spectrometer (resolution of 1 nm).

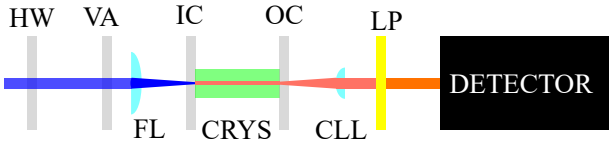

Fig. 4. Schematics of the setup employed for the waveguide laser. HW is the half-wavelength plate, VA is the variable attenuator, FL is the coupling lens, IC is the input coupler, CRYS is the crystal, OC is the output coupler, CLL is the collection lens, LP is the long-pass dielectric filter, and DETECTOR indicates the various instruments employed to analyze the laser beam.

Optics EXPRESS

4.1. Experiments with WG2

The highest values in terms of output power were achieved using waveguide WG2 for all the wavelengths studied. The results, together with the mirrors employed, are summarized in Table 2. Concerning the 523 nm line, we achieved a maximum output power of 65 mW, a slope efficiency of 11% and a threshold pump power of 55 mW with an output coupler transmission of 1%. Data, best fit and intensity profile are reported in Fig. 5(b). The output power at this wavelength was limited by the onset of laser emission at 604 nm at high pump power (P_C>600mW). Regarding the orange (604 nm) emission, we employed an output coupler with an extraction of 16%, reaching a maximum output power of 275 mW, a slope efficiency of 40%, and showing a threshold power of 110 mW. In the end, we observed laser emission at 721 nm. Employing an output coupler with a transmission of 46%, the maximum output power was of 310 mW, the slope efficiency was 50%, and the threshold power was 170 mW. Data, best fits, and intensity profiles are reported in Fig. 5(a). All the observed emissions are π-polarized. The emission spectra of the laser working at the three different wavelengths are summarized in Fig. 6.

Table 2. Summary of the laser results achieved using WG2. P_{THR} is the threshold power, η_c is the slope efficiency and P_{MAX} is the maximum output power of the waveguide laser

λ[nm]	IC	OC	P_{THR}[mW]	η_c[%]	P_{MAX}[mW]	M_x^2	M_y^2
523	1	3	55	11	65	2	2.7
604	2	4	110	40	275	3	3
721	2	5	170	50	310	3	3

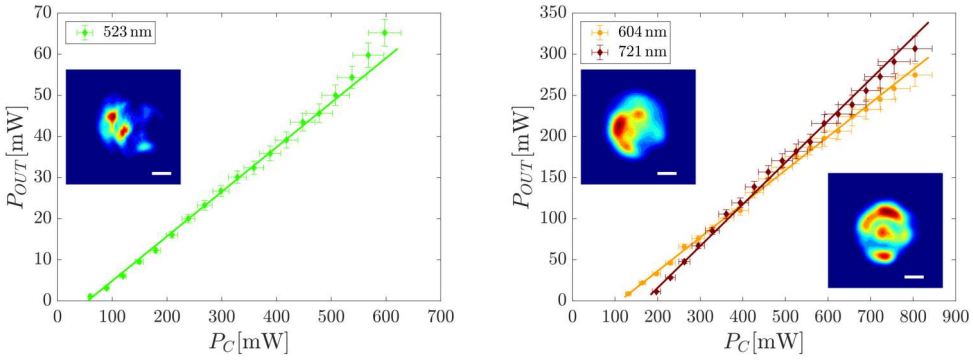

(a) 523 nm.

(b) 721 nm (left inset) and 604 nm (right one).

Fig. 5. Data, best fit, and intensity profile for the laser emission from WG2. The intensity profiles were recorded at maximum output power. The scale bar in the insets corresponds to 10 µm.

4.2. Experiments with WG1

Concerning the emission from WG1, we achieved single-transverse-mode emission at 721 nm, in a TEM_{00}-like mode. The maximum output power was 28 mW, while a slope efficiency of 47% was observed, with a corresponding threshold power of 70 mW. To obtain this result, we used an output coupler with a transmission of 46%. It is possible to set an upper limit on the propagation losses starting from the value of the slope efficiency, as reported in [25]. From the value of 47% slope efficiency at 721 nm, the corresponding limit for propagation losses is 0.5 dB/cm, a more

Optics EXPRESS

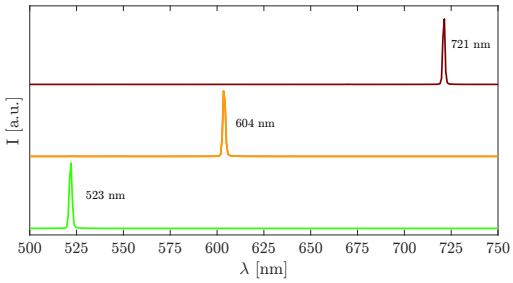

Fig. 6. Spectra of the waveguide laser working at 523 nm, 604 nm, and 721 nm. The resolution of the spectra is equal to 1 nm.

stringent value with respect to the one obtained by coupling and transmission measurement. The values of M^2 were about 1.1 for both the principal axes of the beam.

We also tested laser performance of WG1 at 604 nm, observing the multimodal behavior of the waveguide at this wavelength. Nevertheless, we could achieve a slope efficiency of 50%, although the emission mode was a LP_{11}-like one, Fig. 7. Using an extraction of 16%, the maximum output power achieved was 32 mW, and the threshold was 60 mW. The complete list of the laser results and the corresponding sets of mirrors employed are listed in Table 3. All the emissions are π-polarized. Data, best fit, and intensity profiles are reported in Fig. 7.

Table 3. Summary of the laser results achieved using WG1. P_{THR} is the threshold power, η_C is the slope efficiency and P_{MAX} is the maximum output power of the waveguide laser

λ[nm]	IC	OC	P_{THR}[mW]	η_c[%]	P_{MAX}[mW]	M_x^2	M_y^2
604	2	4	60	50	32	2	1.1
721	2	5	70	47	28	1.1	1.1

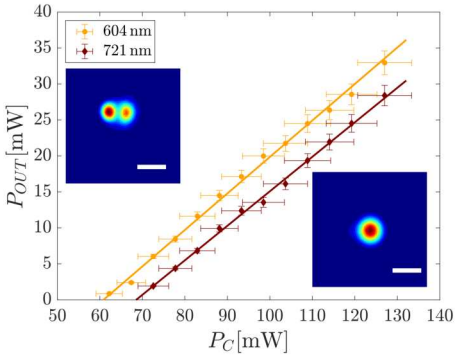

Fig. 7. Data and best fit for the laser emission achieved with WG1. The inset on the left reports the emission at 604 nm while the one on the right reports the 721 nm one. The intensity profiles were both recorded at maximum output power. The scale bar corresponds to 10 µm.

5. Conclusion

In conclusion, we realized a high efficiency diode-pumped Pr-based waveguide laser, reaching output powers of about 275 mW at 604 nm and 310 mW at 721 nm. These values are the highest

Optics EXPRESS

achieved in the literature for diode pumped waveguide lasers [13–15]. By exploiting the greater overlap efficiency between pump beam and laser mode, we reached slope efficiencies of about 50% for both wavelengths, values comparable with those obtained in lasers based on bulk Pr-doped fluoride crystals [3], a result never reported previously for Pr-based waveguide lasers. Moreover, we also demonstrated the first diode-pumped lasing from a single mode waveguide at 721 nm, reaching an output power of 28 mW while maintaining an M^2 lower than 1.1 for both principal axes of the beam. A compact waveguide laser with a diffraction limited beam can be easily included in a more complex device, due to the high quality of the output. In the end, this is the first demonstration of diode-pumped green lasing in a Pr-based waveguide laser, with a slope efficiency of 11% and a maximum output power of 65 mW, the highest values for output power and slope efficiencies and the lowest threshold among all the green emitting CW Pr-based waveguide lasers [12,26]. A more compact single-element laser cavity can be realized in the future by applying a dielectric coating on the crystal facets, obtaining thus a stable monolithic laser with diffraction limited beam, opening the door to possible insertion of the laser source in more complex or metrological devices.

Funding. Ministerio de Ciencia, Innovación y Universidades (PID2020-119818); Consejería de Educación, Junta de Castilla y León (SA136P20).

Acknowledgments. The authors would like to acknowledge Dr. C. Kränkel for the dielectric mirrors employed for the realization of the green laser emission.

Disclosures. The authors declare no conflicts of interest.

Data availability. Data underlying the results presented in this paper are not publicly available at this time but may be obtained from the authors upon reasonable request.

References

1. R. Matthey, C. Affolderbach, and G. Mileti, "Methods and evaluation of frequency aging in distributed-feedback laser diodes for rubidium atomic clocks," Opt. Lett. **36**(17), 3311–3313 (2011).
2. C. Kränkel, D.-T. Marzahl, F. Moglia, *et al.*, "Out of the blue: semiconductor laser pumped visible rare-earth doped lasers," Laser Photonics Reviews **10**(4), 548–568 (2016).
3. H. Tanaka, S. Kalusniak, M. Badtke, *et al.*, "Visible solid-state lasers based on Pr3+ and Tb3+," Prog. Quantum Electron. **84**, 100411 (2022).
4. A. Sottile, E. Damiano, A. D. Lieto, *et al.*, "Diode-pumped solid-state laser platform for compact and long-lasting strontium-based optical clocks," Opt. Lett. **44**(3), 594–597 (2019).
5. K. M. Davis, K. Miura, N. Sugimoto, *et al.*, "Writing waveguides in glass with a femtosecond laser," Opt. Lett. **21**(21), 1729–1731 (1996).
6. A. G. Okhrimchuk, A. V. Shestakov, I. Khrushchev, *et al.*, "Depressed cladding, buried waveguide laser formed in a YAG:Nd3+ crystal by femtosecond laser writing," Opt. Lett. **30**(17), 2248–2250 (2005).
7. E. Kifle, P. Loiko, X. Mateos, *et al.*, "Femtosecond-laser-written hexagonal cladding waveguide in Tm:KLu(WO4)2: μ-Raman study and laser operation," Opt. Mater. Express **7**(12), 4258–4268 (2017).
8. T. Calmano, A.-G. Paschke, S. Müller, *et al.*, "Curved Yb:YAG waveguide lasers, fabricated by femtosecond laser inscription," Opt. Express **21**(21), 25501–25508 (2013).
9. J. E. Bae, T. Calmano, C. Kränkel, *et al.*, "Controllable dynamic single- and dual-channel graphene q-switching in a beam-splitter-type channel waveguide laser," Laser Photonics Reviews **16**(4), 2100501 (2022).
10. J. E. Bae, X. Mateos, M. Aguiló, *et al.*, "Multi-gigahertz mode-locked femtosecond yb:kluw waveguide lasers," Photon. Res. **10**(11), 2584–2589 (2022).
11. T. Calmano, J. Siebenmorgen, F. Reichert, *et al.*, "Crystalline Pr:SrAl12O19 waveguide laser in the visible spectral region," Opt. Lett. **36**(23), 4620–4622 (2011).
12. F. Reichert, T. Calmano, S. Müller, *et al.*, "Efficient visible laser operation of Pr,Mg:SrAl12O19 channel waveguides," Opt. Lett. **38**(15), 2698–2701 (2013).
13. S. Müller, T. Calmano, P. Metz, *et al.*, "Femtosecond-laser-written diode-pumped Pr:LiYF4 waveguide laser," Opt. Lett. **37**(24), 5223–5225 (2012).
14. H. Liu, S. Luo, B. Xu, *et al.*, "Femtosecond-laser micromachined Pr:YLF depressed cladding waveguide: Raman, fluorescence, and laser performance," Opt. Mater. Express **7**(11), 3990–3997 (2017).
15. Y. Ren, Z. Cui, L. Sun, *et al.*, "Laser emission from low-loss cladding waveguides in pr:ylf by femtosecond laser helical inscription," Chin. Opt. Lett. **20**(12), 122201 (2022).
16. D. Baiocco, I. Lopez-Quintas, J. R. V. de Aldana, *et al.*, "Diode-pumped visible lasing in femtosecond-laser-written Pr:LiLuF4 waveguide," Opt. Lett. **48**(7), 1734–1737 (2023).

Optics EXPRESS

17. D. Baiocco, I. Lopez-Quintas, J. R. Vázquez de Aldana, *et al.*, "Comparative Performance Analysis of Femtosecond-Laser-Written Diode-Pumped Pr:LiLuF4 Visible Waveguide Lasers," Photonics **10**(4), 377 (2023).
18. F. Cornacchia, A. Richter, E. Heumann, *et al.*, "Visible laser emission of solid state pumped LiLuF4:Pr3+," Opt. Express **15**(3), 992–1002 (2007).
19. R. L. Aggarwal, D. J. Ripin, J. R. Ochoa, *et al.*, "Measurement of thermo–optic properties of Y3Al5O12, Lu3Al5O12, YAIO3, LiYF4, LiLuF4, BaY2F8, KGd(WO4)2, and KY(WO4)2 laser crystals in the 80–300K temperature range," J. Appl. Phys. **98**(10), 103514 (2005).
20. A. A. Kaminskii, K. ichi Ueda, and N. Uehara, "New Laser-Diode-Pumped CW Laser Based on Nd^{3+}-Ion-Doped Tetragonal $LiLuF_4$ Crystal," Jpn. J. Appl. Phys. **32**(4B), L586–L588 (1993).
21. B. M. Walsh, N. P. Barnes, M. Petros, *et al.*, "Spectroscopy and modeling of solid state lanthanide lasers: Application to trivalent Tm3+ and Ho3+ in YLiF4 and LuLiF4," J. Appl. Phys. **95**(7), 3255–3271 (2004).
22. F. Chen and J. R. V. de Aldana, "Optical waveguides in crystalline dielectric materials produced by femtosecond-laser micromachining," Laser Photonics Reviews **8**(2), 251–275 (2014).
23. X. Sun, S. Sun, C. Romero, *et al.*, "Femtosecond laser direct writing of depressed cladding waveguides in Nd:YAG with ear-like; structures: fabrication and laser generation," Opt. Express **29**(3), 4296–4307 (2021).
24. Y. Morova, B. Morova, H. Jahangiri, *et al.*, "Femtosecond laser written continuous-wave Nd3+:BaY2F8 waveguide laser at 1.3," Opt. Mater. **134**, 113199 (2022).
25. P. W. Metz, F. Reichert, F. Moglia, *et al.*, "High-power red, orange, and green Pr3+:LiYF4 lasers," Opt. Lett. **39**(11), 3193–3196 (2014).
26. A. Baillard, P. Loiko, C. Romero, *et al.*, "Orange surface waveguide laser in Pr:LiYF4 produced by a femtosecond laser writing," Opt. Lett. **48**(23), 6212–6215 (2023).